nature materials

SUPPLEMENTARY INFORMATION

DOI: 10.1038/NMAT4205

Light-emitting diodes by band-structure engineering in van der Waals heterostructures

F. Withers[1], O. Del Pozo Zamudio[2], A. Mishchenko[1], A. P. Rooney[3], A. Gholinia[3], K. Watanabe[4], T. Taniguchi[4], S. J. Haigh[3], A. K. Geim[5], A. I. Tartakovskii[2], K. S. Novoselov[1]

[1]*School of Physics and Astronomy, University of Manchester, Oxford Road, Manchester, M13 9PL, UK*

[2]*Department of Physics and Astronomy, University of Sheffield, Sheffield S3 7RH, UK*

[3]*School of Materials, University of Manchester, Oxford Road, Manchester, M13 9PL, UK*

[4]*National Institute for Materials Science, 1-1 Namiki, Tsukuba 305-0044, Japan*

[5]*Manchester Centre for Mesoscience and Nanotechnology, University of Manchester, Oxford Road, Manchester, M13 9PL, UK*

© 2015 Macmillan Publishers Limited. All rights reserved

DOI: 10.1038/NMAT4205

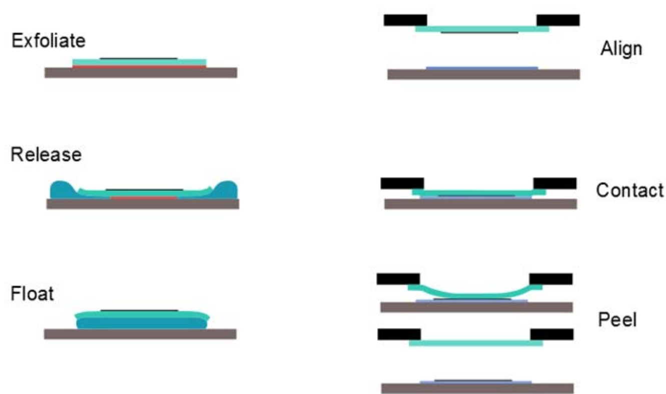

Fig. S1. *Schematic procedure for the 'peel' process.*

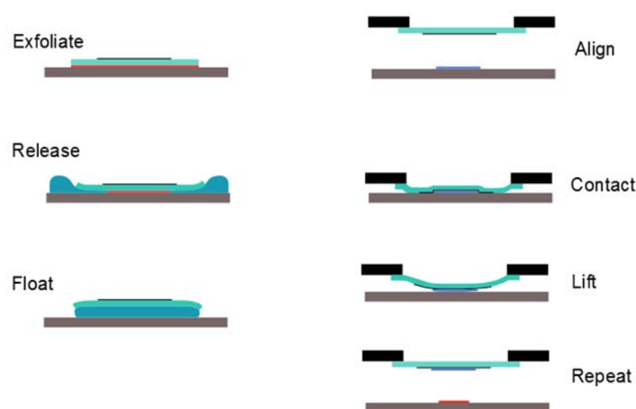

Fig. S2. *Schematic procedure for the 'lift' process.*

S1. Heterostructure preparation

The quantum well (QW) heterostructures were produced via multiple 'peel' and 'lift' transfer processes as described previously in [1, 2]. Fig. S1 and Fig. S2 show the schematic for the processes. For the 'peel' process a flake is mechanically exfoliated onto a polymer double layer then the bottom polymer is dissolved releasing the membrane which then floats on top of the liquid. The PMMA membrane is then inverted and aligned onto the target crystal. The two crystals are brought into contact and heated until the PMMA adheres to the target substrate. Once the flake has adequately stuck to the target crystal the PMMA membrane is brought back. The flake due to the strong Van der Waals interaction peels from the PMMA onto the target flake.

For the 'lift' process the membrane is produced in the same way as shown in Fig. S1. Instead of peeling the flake onto the target crystal, a large flake on the membrane is used to collect a smaller flake on the substrate. The flake to be lifted is exfoliated onto a second thermally oxidised silicon wafer.

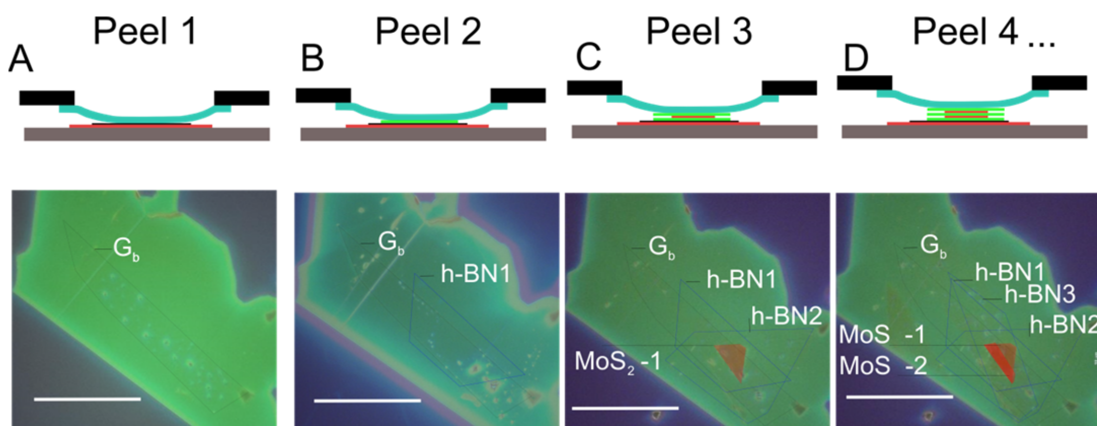

Fig. S3. **(A-D)** *Schematic and differential interference contrast microscope images with semi-transparent dark field images overlaid to highlight flake edges, for the multiple QW structures. Scale bar is 50 µm.*

© 2015 Macmillan Publishers Limited. All rights reserved

Fig. S3 shows the fabrication route for the multiple QW (MQW) structure. Firstly a graphene flake is peeled from a PMMA membrane to a hBN crystal on the Si/SiO_2 substrate, Fig. S3A. After this a thin h-BN tunnel barrier is peeled from the PMMA membrane onto the hBN-Gr_B structure, Fig. S3B. A thin hBN spacer carrying a single layer TMDC crystal (lifted from a second substrate) is then peeled from the membrane, thus completing the first well, Fig. S3C. This process can be repeated as shown in Fig. S3D to produce a double QW and even further to produce triple and quadruple QW structures.

S2. Data for additional devices

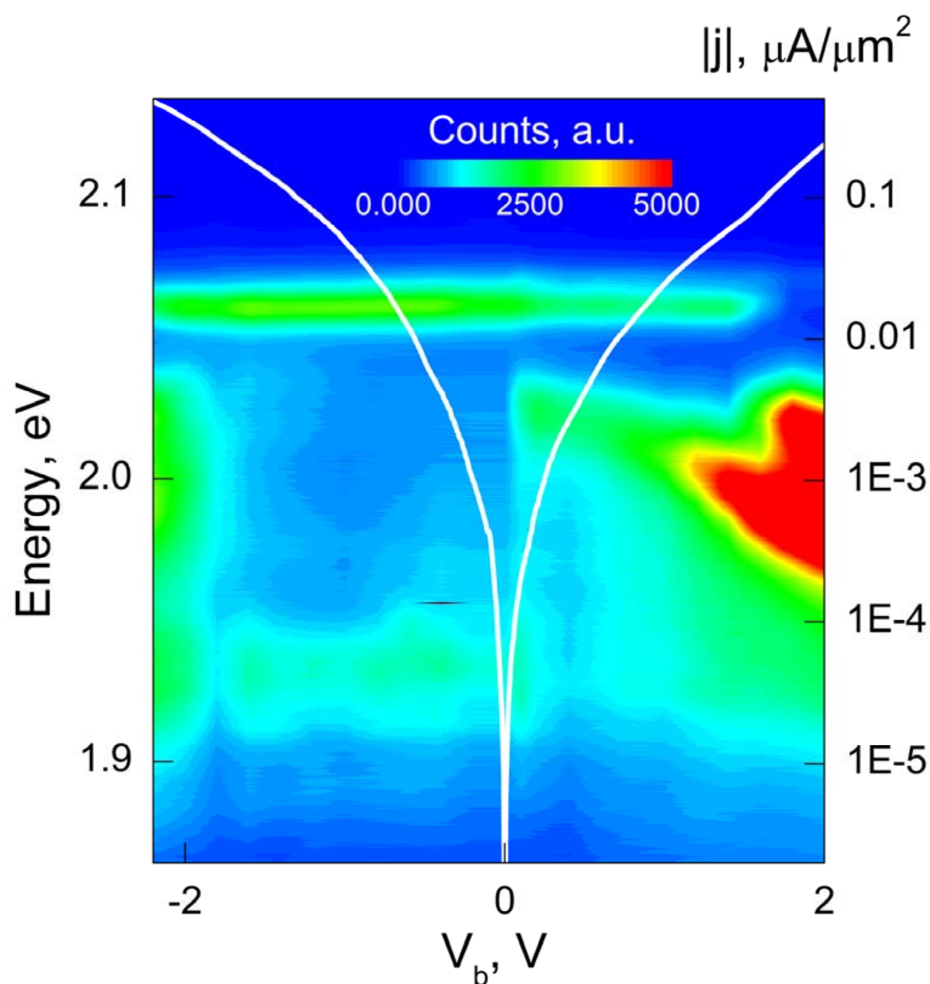

Fig. S4. ***(A)*** *Colour map of the PL for the WS_2 quantum well shown in Figure 2 of the main text E_L = 2.33 eV .*

© 2015 Macmillan Publishers Limited. All rights reserved

DOI: 10.1038/NMAT4205

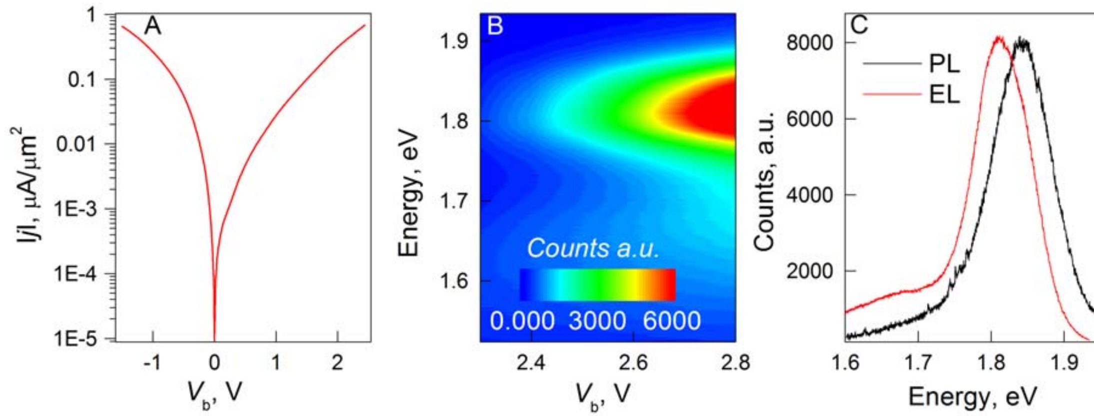

Fig. S5. ***(A)*** *|j|-V_b characteristics for another SQW made from single layer MoS_2.* ***(B)*** *Colour plot of the EL intensity vs bias voltage for the same device.* ***(C)*** *The normalised EL and PL spectra.*

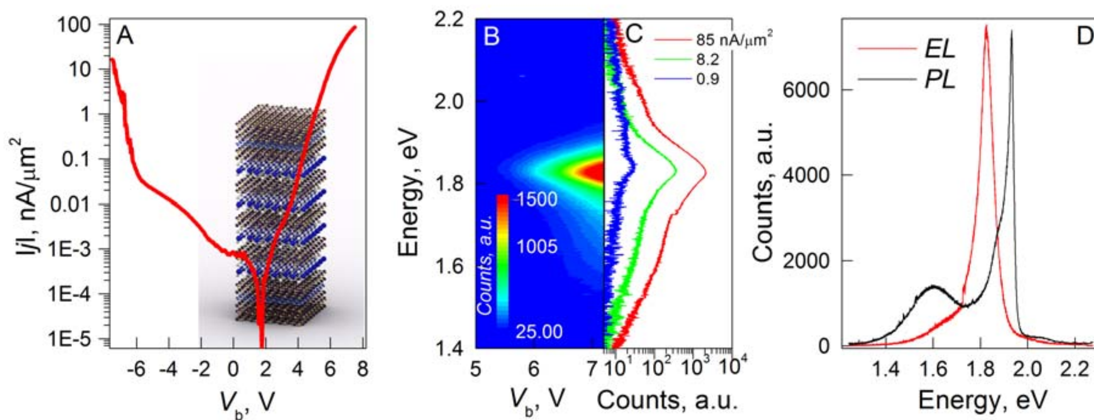

Fig. S6. ***(A)*** *|j|-V_b characteristics for a device with four QW each made of single layer MoS_2. Inset: an image of the approximate structure.* ***(B)*** *Colour map of the EL spectrum.* ***(C)*** *EL spectra for a few different injection currents showing the onset of EL.* ***(D)*** *The EL and PL for the same device (normalised).*

© 2015 Macmillan Publishers Limited. All rights reserved

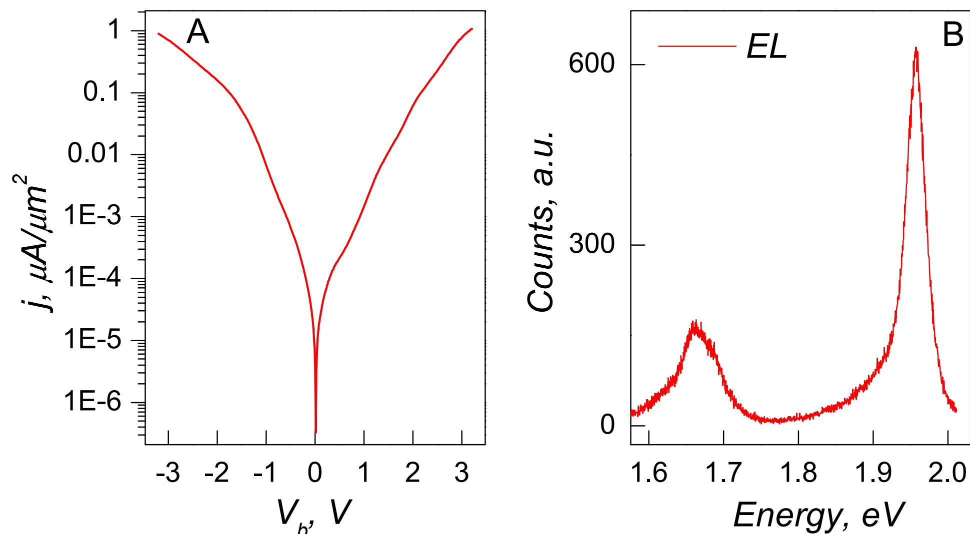

Fig. S7. ***(A)*** *|j|-V_b characteristics for the bilayer WS_2 device described in the main text* ***(B)*** *Single spectrum of the electroluminescence at T = 6 K at a bias voltage of 3.2 V.*

Device	EL peak position, eV	FWHM, meV	QE at highest injection current and T = 6 K, %
SL MoS_2 – 1	1.86	30	0.30
SL MoS_2 – 2	1.81	90	0.51
FL MoS_2	1.86	34	0.06
SL WS_2	2.00	23	1.32
BL WS_2	1.96	29	0.09
3MQW MoS_2	1.94	78	6.00
4MQW MoS_2	1.83	65	8.40
WSe_2 / MoS_2 2QW-1	1.66	14	4.80
WSe_2 / MoS_2 2QW-2	1.68	21	5.40

Table S1. *The main peak position, width and quantum efficiency for the electroluminescence spectra for different devices based of TMDC materials.*

© 2015 Macmillan Publishers Limited. All rights reserved

DOI: 10.1038/NMAT4205

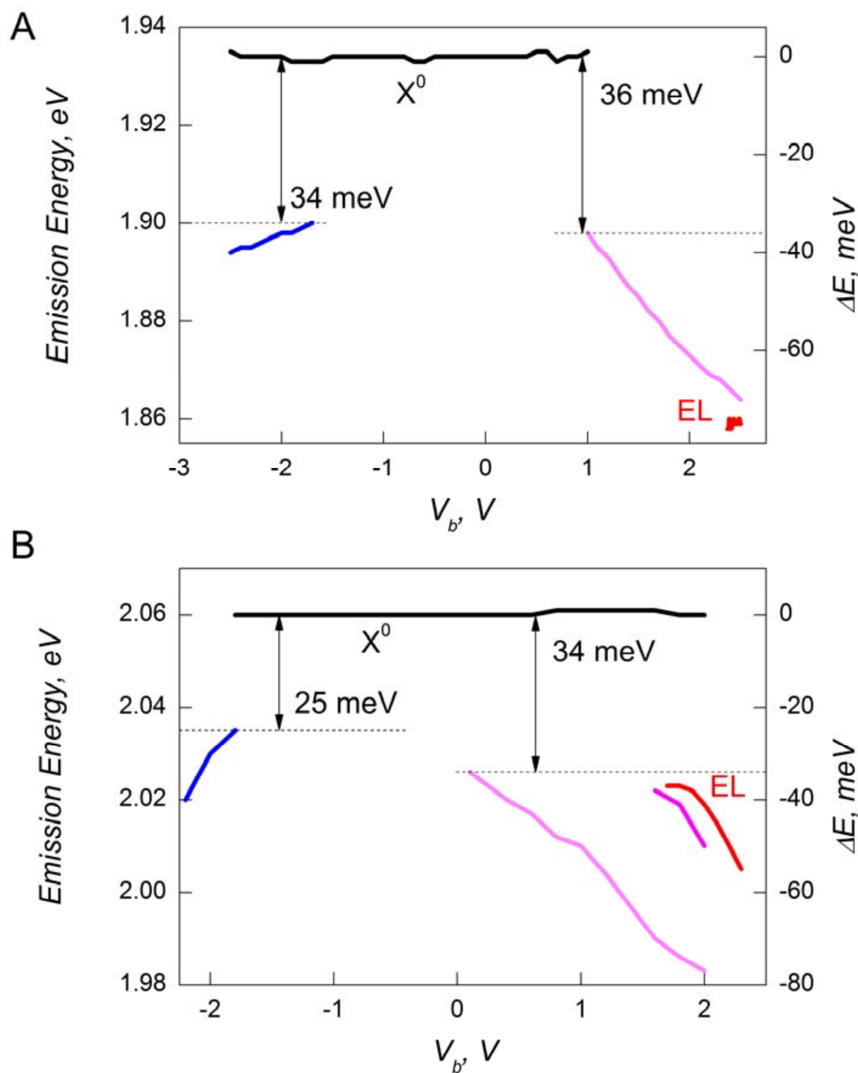

Fig. S8. *Extracted peak positions vs bias voltage for* ***(A)*** *MoS_2,* ***(B)*** *WS_2.*

© 2015 Macmillan Publishers Limited. All rights reserved

S4. Quantum efficiency

The quantum efficiency is defined as the number of photons emitted per number of injected electron-hole pairs $N2e/i$ (N = number of emitted photons per second, e electron charge, i is the current passing through a 2 micron area which is our collection area determined by the slit). In order to estimate the number of emitted photons we need to estimate our collection efficiency. The total loss is defined as,

$\eta = \eta_{Lens}\eta_{optic}\eta_{system}$.

η_{optic} is the loss of all the optical components in the optical circuit. It was measured directly using a 1.96 eV laser and a power meter to determine the loss at each component. We find $\eta_{optic} = 0.18$.

η_{system} - converts the number of photons arriving at the incoming slit of the detector into the detector counts. It takes into account the loss of photons which pass through the slit, grating and onto the CCD and has been again measured directly by using the 1.96 eV laser and taking spectra of the laser for different powers in order to get a counts vs incident photons. For our system we get 4203 integrated cts/sec per 1 pW. If the system were 100% efficient we should count N=P/hv=3177476 photons, therefore we arrive at an estimate for the system efficiency to be η_{system}=4203/3177476 =1.32 x 10^{-3}.

η_{Lens} is the efficiency of the lens collection[3]. We use a 50x objective with a numerical aperture, NA = 0.55. The TMDC layer is effectively encapsulated within hBN of refractive index n = 2.2[4].

$$\eta_{Lens} = \frac{1}{4\pi}\int_0^{2\pi} d\varphi \int_0^{\arcsin(\frac{NA}{n})} d\theta sin\theta = \frac{1}{2}\left[1 - \sqrt{1 - \left(\frac{NA}{n}\right)^2}\right] = 0.016$$

From this we can make an estimate of the quantum efficiency to be, $QE = {}^{2eN_{counts}}/_{\eta i}$. In this equation N_{counts} is the integrated number of counts taken for the spectrum.

© 2015 Macmillan Publishers Limited. All rights reserved

 DOI: 10.1038/NMAT4205

S5. Cross sectional imaging

Details of cross sectional imaging of heterostructures produced from 2D materials can be found in [5].

S5.1 Preparation of cross sectional STEM samples

A dual beam instrument (FEI Dual Beam Nova 600i) has been used for site specific preparation of cross sectional samples suitable for TEM analysis using the lift-out approach [Schaffer, M. *et al.* Sample preparation for atomic-resolution STEM at low voltages by FIB [6]]. This instrument combines a focused ion beam (FIB) and a scanning electron microscope (SEM) column into the same chamber and is also fitted with a gas-injection system to allow local material deposition and material-specific preferential milling to be performed by introducing reactive gases in the vicinity of the electron or ion probe. The electron column delivers the imaging abilities of the SEM and is at the same time less destructive than FIB imaging. SEM imaging of the device prior to milling allows one to identify an area suitable for side view imaging. After sputtering of a 10 nm carbon coating and then a 50 nm Au- Pd coating on the whole surface ex-situ, the Au/Ti contacts on graphene were still visible as raised regions in the secondary electron image. These were used to correctly position and deposit a Pt strap layer on the surface at a chosen location, increasing the metallic layer above the device to ~2 µm. The Pt deposition was initially done with the electron beam at 5kV e^- and 1nA up to about 0.5µm in order to reduce beam damage and subsequently with the ion beam at 30kV Ga^+ and 100pA to build up the final 2µm thick deposition. The strap protects the region of interest during milling as well as providing mechanical stability to the cross sectional slice after its removal. Trenches were milled around the strap by using a 30 kV Ga^+ beam with a current of 1-6nA, which resulted in a slice of about 1µm thick. Before removing the final edge supporting the milled slice and milling beneath it to free from the substrate, one end of the Pt strap slice was welded to a nanomanipulator needle using further Pt deposition. The cross sectional slice with typical dimensions of 1 µm x 5 µm x 10 µm could then be extracted and transferred to an Omniprobe copper half grid as required for TEM. The slice was then welded onto the grid using Pt deposition so that it could be safely separated from the nanomanipulator by FIB milling. The lamella was further thinned to almost electron beam transparency using a 30kV Ga^+ beam and 0.1-1nA. A final gentle polish with Ga+ ions (at 5kV and 50pA) was used to remove side damage and reduce the specimen thickness to 20-70nm. The fact that the cross sectional slice was precisely extracted from the chosen spot was confirmed for all devices by comparing the positions of identifiable features such as Au contacts and /or hydrocarbon bubbles, which are visible both in the SEM images of the original device and within TEM images of the prepared cross section.

© 2015 Macmillan Publishers Limited. All rights reserved

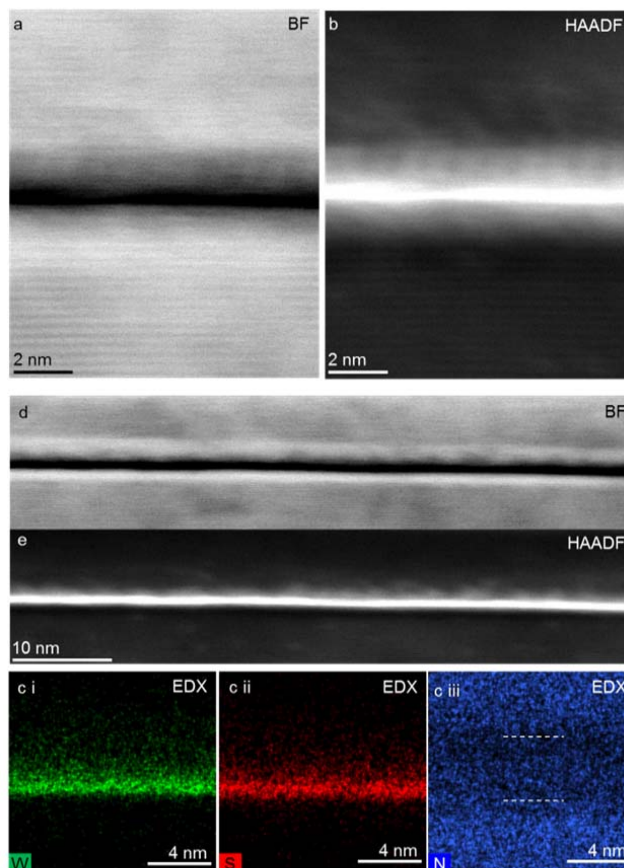

Fig. S9. *Bright field (a) and high angle annular dark field (b) STEM images of a single layer WS_2 heterostructure cross-section. WS_2 lattice fringes are visible in both images, as are the boron nitride fringes at a lower intensity. (c i-iii) Elemental maps for W, S and N extracted from energy dispersive x-ray (EDX) spectrum image data. The top and bottom graphene electrodes can be seen as deficiencies in the nitrogen EDX map (see dashed white lines). This allows the number of boron nitride layers between the graphene and WS_2 layer above and below the WS_2 layer to be estimated as five and two layers respectively. (d) and (e) show BF and HAADF images at lower magnification.*

S5.2 Scanning transmission electron microscope imaging and energy dispersive x-ray spectroscopy analysis

High resolution scanning transmission electron microscope (STEM) imaging was performed using a probe side aberration-corrected FEI Titan G2 80-200 kV with an X-FEG electron source operated at 200kV. High angle annular dark field (HAADF) and bright field (BF) STEM imaging was performed using a probe convergence angle of 26 mrad, a HAADF inner angle of 52 mrad and a probe current of ~200 pA. Energy dispersive x-ray (EDX) spectrum imaging was performed in the Titan using a Super-X four silicon drift EDX detector system with a total collection solid angle of 0.7 srad. The multilayer structures were oriented along an <hkl0> crystallographic direction by taking advantage of the Kukuchi bands of the Si substrate.

© 2015 Macmillan Publishers Limited. All rights reserved

DOI: 10.1038/NMAT4205

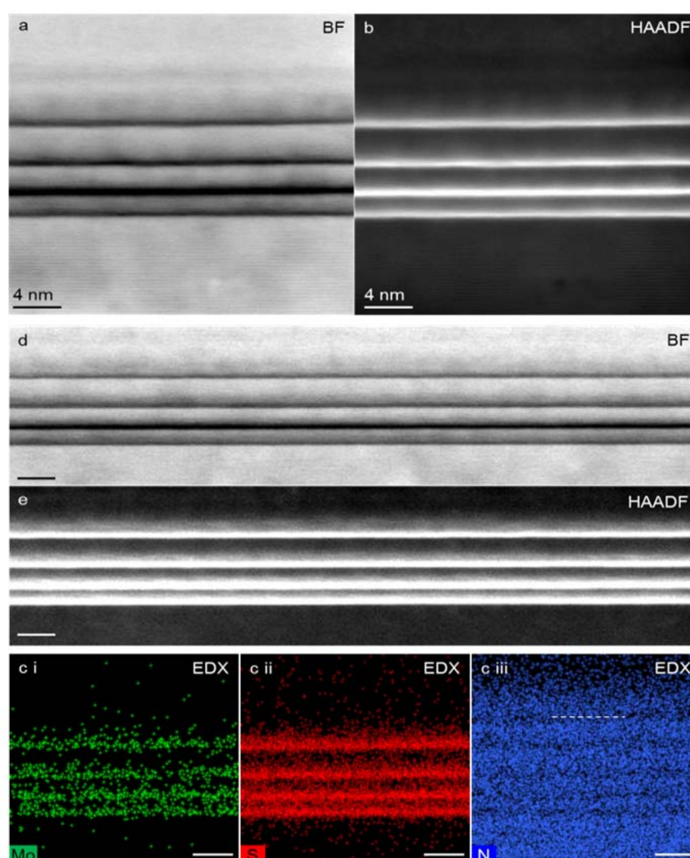

Fig. S10. *Cross sectional Imaging of MoS2 multilayer quantum well. (a) Bright field and (b) high angle annular dark field STEM images of the four layer MoS_2 heterostructure cross-section. Boron nitride lattice fringes are clearly visible in both images, as are the position of the MoS_2 monolayers. The number of boron nitride layers between each MoS_2 monolayer were determined to be four, six and nine layers for the bottom, middle and top stacks respectively. (c i-iii) Show elemental maps for Mo, S and N extracted from energy dispersive x-ray (EDX) spectrum image data. The top graphene electrode can be seen as a deficiency in the nitrogen EDX map (indicated by dashed white line in (f)). This allows the number of boron nitride layers between the top MoS_2 layer and the graphene to be estimated as seven layers. (d) and (e) show BF and HAADF images at lower magnification. The structure was found to be atomically flat and highly uniform over regions >100nm. All scale bars are 4 nm.*

References

1. Wang, L., et al., *One-Dimensional Electrical Contact to a Two-Dimensional Material.* Science, 2013. **342**(6158): p. 614-617.
2. Kretinin, A.V., et al., *Electronic quality of graphene on different atomically flat substrates.* arXiv:1403.5225, 2014.
3. Mueller, T., et al., *Efficient narrow-band light emission from a single carbon nanotube p-n diode.* Nature Nanotechnology, 2010. **5**(1): p. 27-31.
4. Gorbachev, R.V., et al., *Hunting for monolayer boron nitride: optical and Raman signatures.* Small, 2011. **7**(4): p. 465-468.
5. Haigh, S.J., et al., *Cross-sectional imaging of individual layers and buried interfaces of graphene-based heterostructures and superlattices.* Nature Materials, 2012. **11**(9): p. 764–767.
6. Schaffer, M., B. Schaffer, and Q. Ramasse, *Sample preparation for atomic-resolution STEM at low voltages by FIB.* Ultramicroscopy, 2012. **114**: p. 62-71.

© 2015 Macmillan Publishers Limited. All rights reserved